Am J Cancer Res 2023;13(4):1363-1376
www.ajcr.us /ISSN:2156-6976/ajcr0148793

Original Article

EBNA2 mediates lipid metabolism and tumorigenesis through activation of ATF4 pathway

Jia Feng, Ping Zhang, Paul Yao, Hongyu Zhang

Department of Hematology, Peking University Shenzhen Hospital, Shenzhen 518036, Guangdong, P. R. China

Received December 27, 2022; Accepted March 9, 2023; Epub April 15, 2023; Published April 30, 2023

Abstract: Epstein-Barr virus (EBV) can infect the majority of the human population with no obvious symptoms and is associated with tumor development, although the mechanism is still largely unknown. In this study, we investigated the role and the underlying mechanism of EBV nuclear antigen 2 (EBNA2) in tumorigenesis. We found that the infection of EBNA2 in human B lymphocytes (HBL) upregulated the expression of activating transcription factor 4 (ATF4). Furthermore, we used gene expression or knockdown approach to demonstrate the effect of EBNA2 on redox balance, mitochondrial function, lipid metabolism, and cell proliferation in both HBL and EBV-transformed lymphocyte cell line (LCL). More importantly, we applied *in vivo* xenograft tumor mouse model to explore the contribution of EBNA2 and ATF4 in tumor growth and mouse survival. Mechanistically, we revealed that EBNA2 exposure caused persistent expression of ATF4 via EBNA2-mediated epigenetic changes, which increased the binding ability of upstream stimulating factor 1 (USF1) on the ATF4 promoter. ATF4 activation in HBL cells modulated the expression of lipid metabolism-related genes and potentiated fatty acid oxidation and lipogenesis. Conversely, knockdown of either EBNA2 or ATF4 in LCL suppressed lipid metabolism, modulated redox balance and mitochondrial function, as well as inhibited tumor cell proliferation. In consistent with these findings from in vitro study, an *in vivo* xenograft model confirmed that knockdown of either EBNA2 or ATF4 inhibited the gene expression of SREBP1, ChREBP, and FAS, as well as suppressed tumor growth and prolonged animal survival. Collectively, this study demonstrates that EBNA2 mediates tumorigenesis through ATF4 activation and the modulation of lipid metabolism; therefore, our findings provide a novel avenue for the clinical treatment of EBV-mediated cancer.

Keywords: EBV, EBNA2, lipid metabolism, ATF4 and USF1

Introduction

Epstein-Barr virus (EBV) has been reported to be associated with a variety of tumors, including nasopharyngeal carcinoma and nasal Nature/Killer/T-cell lymphoma NKTCL [1, 2]. Most of the human population has latent EBV infection but usually shows no obvious symptoms [3]. It has been reported that EBV infection may cause tumorigenesis through EBV-encoded oncogenic proteins such as EBV nuclear antigen 2 (EBNA2) 1 [4, 5]. As a transcription factor, EBNA2 plays a critical role in EBV-mediated cell transformation and tumorigenesis [6-8] by activating multiple latent viral and cellular genes, including Latent Membrane Protein 1 (LMP1) and Myc [9-11]. Intriguingly, recent studies have also shown that EBNA2 regulates gene expression through epigenetic changes [12-15] with metabolic rearrangement toward aerobic glycolysis, thereby contributing to tumorigenesis [16], although the detailed mechanism is largely unknown.

Activating transcription factor 4 (ATF4) is a stress-mediated transcription factor that is highly expressed in tumors [17-19]. ATF4 upregulation results in a poor prognosis [20-22], and ATF4 is involved in many metabolic processes during tumor development, including glucose metabolism, protein synthase, redox balance, and mitochondrial modulation [23-25]. In addition, ATF4 is involved in mitochondrial fat oxidation [26] and lipid metabolism through the upregulation of fatty acid synthase (FAS), carbohydrate-responsive element-binding protein (ChREBP), and sterol regulatory element-binding protein 1 (SREBP1) [27], although its regulator mechanism remains to be determined.

It has been known that LMP1 plays a central role in EBV modulated lipid metabolism and the

subsequent tumorigenesis [16, 28]. LMP1 regulates lipogenesis through the upregulation of FAS [29] and SREBP1, contributing to cell proliferation and nasopharyngeal carcinoma progression [30]. In addition, EBV and LMP2A affect lipid accumulation and increase the migration of cancer cells [28, 31]. Similarly, EBNA2 and SREBP1 play important roles in the fatty acid pathway to promote B-cell proliferation and survival [32]. However, there are few studies regarding EBV-mediated lipogenesis through ChREBP [33, 34]. Hence, the mechanism of EBV-mediated lipogenesis and its contribution to tumorigenesis require further characterization.

In this study, we investigated the effects as well as the underlying mechanism of EBNA2-mediated lipid metabolism in tumorigenesis. Specifically, we explored the mechanism of transient EBV/EBNA2 exposure-mediated persistent ATF4 activation through *in vitro* study in human B lymphocytes (HBL) via luciferase reporter assay and chromatin immunoprecipitation techniques. Furthermore, the mechanism of ATF4 activation-induced cell growth was investigated through analyzing fatty acid oxidation (FAO) and lipogenesis as well as its target genes such as SREBP1, ChREBP, and FAS. Moreover, the potential modulatory effects on redox balance and mitochondrial function were also determined. Simultaneously, EBV-transformed lymphoblastoid cell lines were employed to evaluate the influence of EBNA2/ATF4 on cancer cell proliferation in vitro and xenograft tumor growth *in vivo* as well as animal survival in a mouse model.

Materials and methods

The full section of the Experimental Procedures can be found in Supplementary Materials, and all primers used for gene knockdown and quantitative PCR were summarized in Table S1.

Reagents and cell lines

Antibodies against ATF4 (sc-390063), ChREBP (sc-515922), FAS (sc-48357), Smad4 (sc-7966), Sp1 (sc-17824), SREBP1 (sc-13551), USF1 (sc-390027), Zic3 (sc-101201) were purchased from SCBT (Beijing, China). Antibodies against EBNA2 (ab90543), HNF3 (ab108422), and SPZ1 (ab235302) were purchased from Abcam. The EBNA2 adenovirus and shEBNA2 lentivirus, as well as the corresponding empty controls, were kindly provided by Dr. Haimou Zhang (Hubei University). shRNA lentivirus particles targeting human ATF4 (sc-35112-V) and USF1 (sc-36783-V) were purchased from SCBT. HBL cells were isolated from healthy human peripheral blood using the EasySep™ Human B Cell Isolation Kit (#17954), while lymphoblastoid cell line 1 (LCL1) was generated by transforming HBL cells with EBV virus infection as described previously [35].

Construction of ATF4 luciferase reporter plasmids

The human ATF4 promoter was identified by Ensembl #: ENST00000337304.2 ATF4-201, amplified (2 kb upstream + 1st exon) by PCR using human B lymphocytes genomic DNA as template, and inserted into pGL3-basic plasmid. The PCR primer sequences were: ATF4 forward primer: 5'-atat-ggtacc-ggg ctc aag caa tcc tcc cac-3' (KpnI) and ATF4 reverse primer: 5'-atat-agatct-cct tgc tgt tgt tgg agg gac-3' (Bgl II). ATF4 promoter deletion/mutation plasmids were also produced by PCR and confirmed by DNA sequencing.

Construction of ATF4/USF1 lentivirus plasmids

The cDNA plasmids expressing human ATF4 and USF1 were obtained from Open Biosystems. Then, the coding sequences of ATF4 and USF1 were amplified using the following primers: ATF4 forward: 5'-atat-gaattc (EcoR1) - agc cat ttc tac ttt gcc cgc-3', ATF4 reverse: 5'-atat-ggatcc (BamH1) - ttt ttt ttt ttt ttt act ttc cct aca-3'; USF1 forward: 5'-atat-gaattc (EcoR1) - gcc cct cac caa cat ggc cgc-3', USF1 forward: 5'-atat-ggatcc (BamH1) - aga taa aat tgt tca aag cca-3'. The amplified cDNA fragments were cloned into the pLVX-Puro vector for lentivirus production.

Methods: Total RNA was extracted by Trizol reagent; mRNA expression was determined by quantitative PCR, and protein levels were determined by western blotting following standard protocols. To investigate EBAN2-regulated ATF4 transcriptional activation, the activity of wild type and mutant ATF4 promoter was measured by luciferase reporter assay. The binding ability of EBAN2 to ATF4 promoter was determined by chromatin immunoprecipitation. To evaluate the redox balance, reactive oxygen species

(ROS) formation was determined using CM-H2DCFDA-based fluorescence. Mitochondrial function was determined through mitochondrial replication, ATP generation, mitochondrial membrane potential (ΔΨm) and apoptosis rate. EBV DNA copy numbers were determined by qPCR of the extracted genomic DNA [36]. The colony formation assay and Ki-67 immunostaining were performed to measure cell growth in vitro using standard protocol. Fatty acid oxidation (FAO) was determined by calculating the oxidation of [^{14}C] palmitate using a previously described method [37]. The redox balance of the tumor tissues was evaluated using the superoxide anion ($O_2^{\cdot-}$) release through the DMSO/TBAC-based chemiluminescence method, as described previously [38].

De novo lipogenesis: Briefly, cells were incubated in serum-free medium with 100 nM insulin at 37°C overnight followed by incubatiion in lipogenesis medium (DMEM medium with 100 nM insulin, 10 μM cold acetate and 0.5 μCi ^{3}H-acetate) at 37°C for 2 h. Cells were then lysed in 120 μl of 0.1 N HCl, and 100 μl of lysates were transferred to a 1.5 ml centrifuge tube for further analysis. An aliquot of 10 μl lysates was used for protein quantification with the Pierce™ BCA Protein Assay Kit according to the manufacturer's instruction. The lipids were extracted by adding 500 μl of 2:1 chloroform-methanol (v/v) followed by 5 min incubation at room temperature (RT). After a brief vortex, 250 μl of water was added to the cell lysates, which was mixed again by vortexing and was incubated at RT for another 5 min. After centrifugation at 3000×g for 10 min at RT, the lower phase was transferred to vial containing 4 ml of liquid scintillation fluid, and ^{3}H activity was determined by the scintillation counter and expressed as counts per minute (cpm) [39].

In vivo mouse experiments: Balb/c athymic nude male mice (6 weeks old) were purchased from Guangdong Medical Animal Center. To generate xenograft tumors, mice were injected via tail vein with 2×10^6 (in 0.1 ml PBS) of 5 different treated LCL1 cells (n=9) as 5 treatment groups: Group 1 (CTL): Cells infected by control (CTL) lentivirus; Group 2 (shEBNA2): Cells infected by shEBNA2 lentivirus; Group 3 (shATF4): Cells infected by shATF4 lentivirus; Group 4 (shUSF1): Cells infected with shUSF1 lentivirus; and Group 5 (shEBNA2/↑ATF4): Cells infected with shEBNA2 and ATF4 lentivirus in the presence of 10 μg/ml puromycin. The experimental mice were monitored daily and euthanized by cervical dislocation when their body weight was reduced by 20% of their initial weight. Tumor tissues were dissected from lung and used for gene expression analysis and *in vivo* superoxide anions ($O_2^{\cdot-}$) release assay [38], as well as were fixed and examined for the number of metastases per lung under a microscope. The tumor spots were imaged by H&E staining and quantified using the 3DHISTECH Pannoramic Viewer.

Results

Overexpression of EBNA2 induced ATF4 upregulation and modulated lipid metabolism

To investigate the effects of EBV/EBNA2 on cellular functions, we first infected hTERT-immortalized HBL cells with EBV or EBNA2 adenovirus and found that EBNA2 mRNA expression was induced from passage 0 and diminished quickly following continuous culture and completely disappeared at passage 6 (**Figure 1A**). Notably, ATF4 mRNA level was significantly increased upon EBV/EBNA2 exposure and remained high until passage 6 (**Figure 1B**). In addition, western blot analysis indicated the ATF4 protein level was consistent with its mRNA level (**Figure 1C**, **1D**). Furthermore, we determined EBV genomic copy number following EBV infection and found that EBV virus diminished quickly following cell culture and disappeared completely at passage 6 (Figure S1A, S1B). After confirming the expression of EBV/EBNA2 in HBL cells, we analyzed the effect of EBV/EBNA2 on lipogenesis-related genes and found that EBV/EBNA2 overexpression significantly increased the protein levels of SREBP1, ChREBP, and FAS (**Figures 1E**, **1F**, S2A) compared with that in the vector infected cells. We also evaluated the effect of EBV/EBNA2 on lipid metabolism and found a significantly increased palmitate oxidation (**Figure 1G**) and de novo lipogenesis (**Figure 1H**). Together, these data suggested that EBNA2 exposure induced ATF4 expression and modulated lipid metabolism in HBL cells.

EBNA2 activated ATF4 through epigenetic modification and subsequently increased USF1 binding on ATF4 promoter

We further explored how EBNA2 activated ATF4 transcription in HBL cells by using luciferase

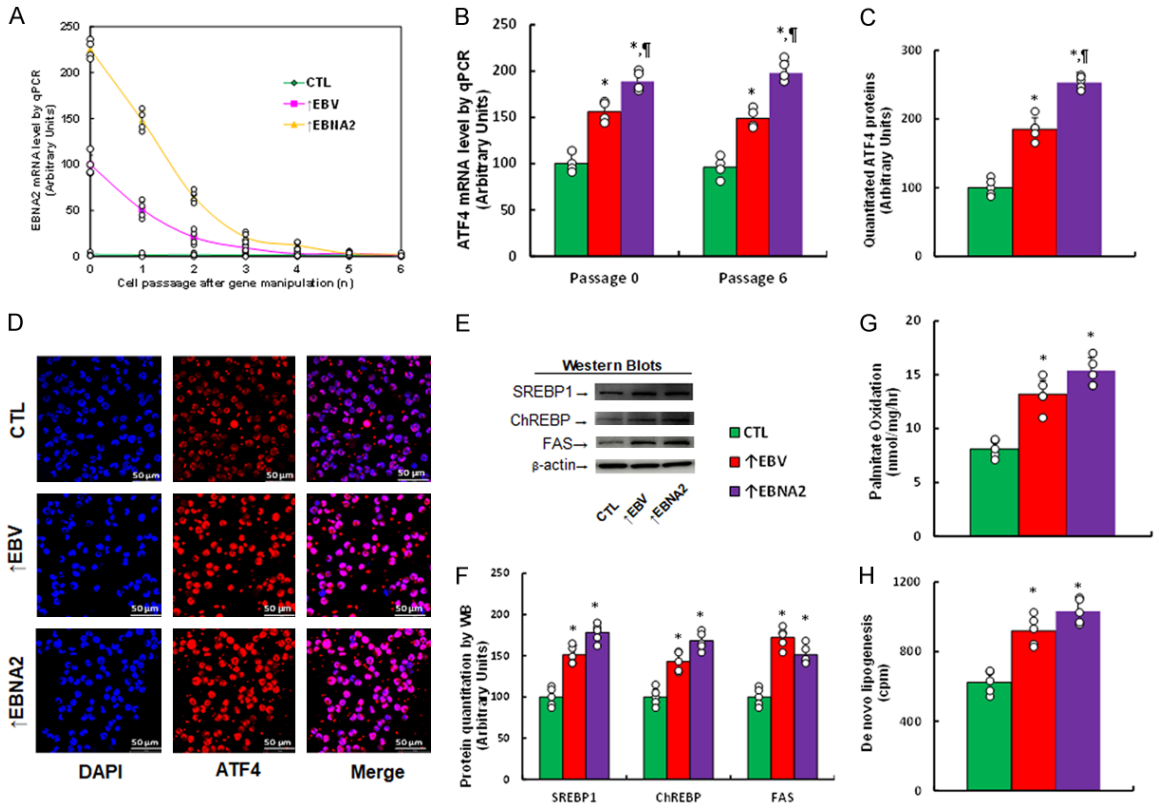

Figure 1. EBNA2 expression induces persistent ATF4 upregulation and modulates lipid metabolism. HBL cells were infected with control (CTL), EBV virus (↑EBV) or EBNA2 adenovirus (↑EBNA2) and analyzed. (A) mRNA levels of EBNA2, n=4. (B) mRNA levels of ATF4, n=4. (C-H) EBV/EBNA2-infected HBL cells were analyzed in passage 6. (C) Quantification of ATF4 protein levels, n=5. (D) Representative western blot of ATF4 for (C). (E) Representative western blots. (F) Quantification of protein levels for (E), n=5. (G) Palmitate oxidation, n=5. (H) De novo lipogenesis, n=5. *, $P<0.05$, vs CTL group; ¶, $P<0.05$, vs EBV group.

reporter assay. We generated a series of ATF4 reporter plasmids with 5'-promoter deletion and infected these mutant constructs individually in HBL cells in the presence of EBNA2 adenovirus infection. Our results showed that ATF4 promoter deletion at -2000, -1600, -1200, -800, -600, -400, -300, -200, and -100 had no effect on EBNA2 activity. However, the reporter activation was completely diminished in the p-ATF4-0 construct containing -100~0 deletion, suggesting that the EBNA2-responsive element on the ATF4 promoter is located in the region of -100~0 (**Figure 2A**). Furthermore, to reveal the binding motif of EBNA2 in ATF4, we performed sequence analysis and identified the following potential binding motifs in this region: USF1 (-89), SPZ1 (-76), Zic3 (-53), HNF3 (-36), Sp1 (-26) and Smad4 (-18) (**Figure 2B**). Then, we generated mutation constructs for each binding motif in the ATF4 full-length reporter plasmid and used luciferase activity assay to examine the activity of these mutants. The results showed that only mutation in USF1 motif (from red to green, **Figure 2B**) completely diminished EBNA2-mediated ATF4 activation, suggesting that EBNA2 activated ATF4 expression through the USF1 binding element (**Figure 2C**). Moreover, we assessed the potential epigenetic modifications in HBL cells and found that EBV and EBNA2 infection significantly decreased H3K9me2 and H3K27me3 modifications compared with that in the control cells, but had no effect on H3K9me3 and H3K27me2 modification (**Figure 2D**). Interestingly, exposure to EBV and EBNA2 did not affect DNA methylation (Figure S3). Importantly, we performed ChIP analysis using the corresponding antibodies to confirm the binding abilities of these motifs and found that treatment with EBV and EBNA2 infection significantly increased USF1 binding, but had no effect on other motifs (**Figure 2E**), consistent with the results of luciferase reporter assay. To determine the functional significance of USF1 on EBNA2 activation of ATF4, we knocked down EBNA2 and USF1 by shEBNA2 and shUSF1, respectively, and found

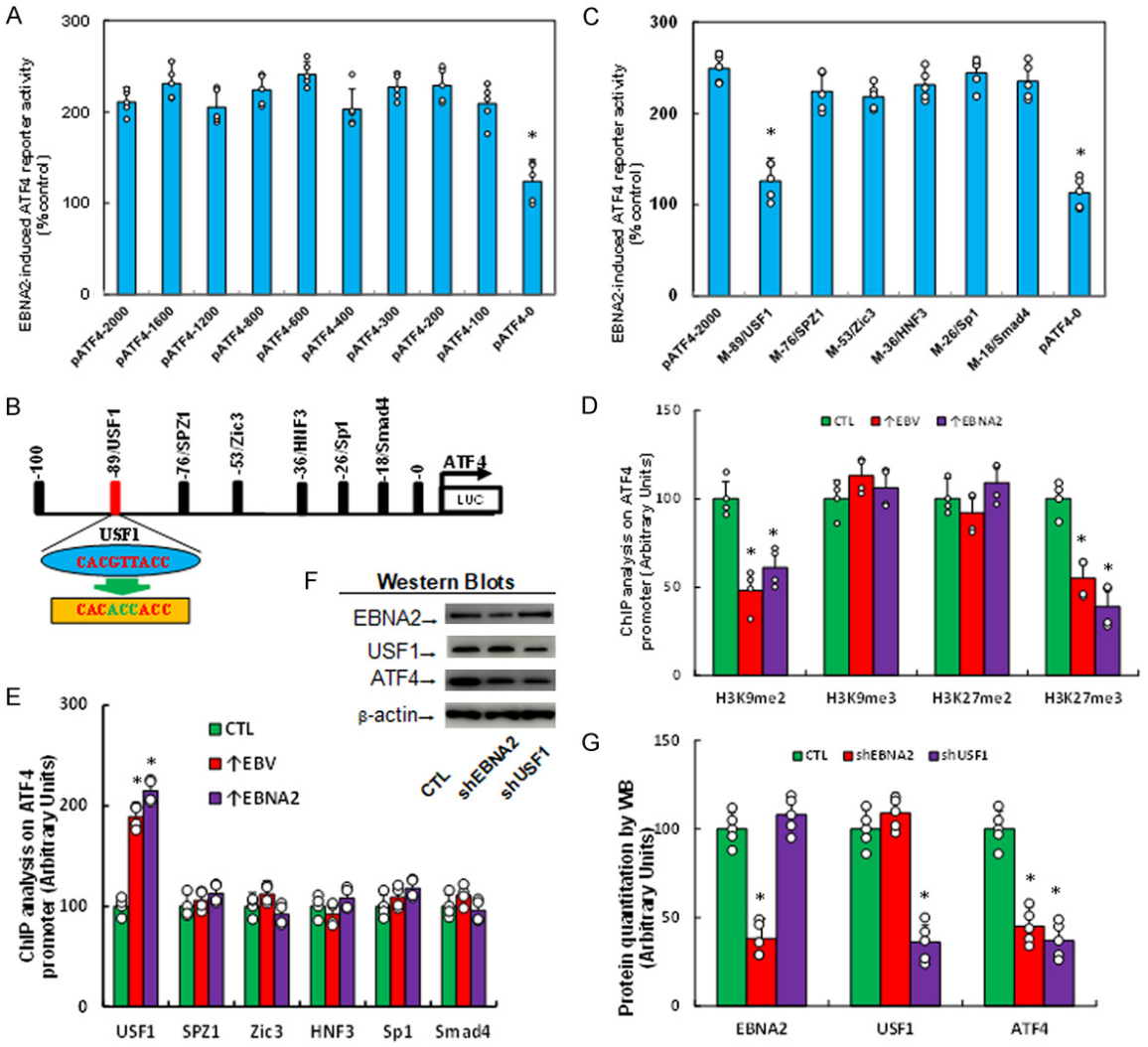

Figure 2. EBNA2 activates ATF4 through epigenetic modification and subsequently increased USF1 binding to the ATF4 promoter. (A-E) The hTERT-immortalized HBL cells were used for promoter mapping and activity assays. (A) Luciferase reporter activities of ATF4 promoter deletion mutants in hTERT-immortalized HBL cells, n=5. *, $P<0.05$, vs pATF4-2000 group. (B) A schematic diagram of binding motifs in the range of -100~0 on the ATF4 promoter. (C) Luciferase activity of ATF4 promoter mutation reporters, n=5. *, $P<0.05$, vs pATF4-2000 group. (D, E) ChIP analysis on ATF4 promoter for H3 methylation (D) and different transcription factors (E), n=4. *, $P<0.05$, vs CTL group. (F, G) EBNA2 or USF1 knockdown in LCL1 cells by either shEBNA2 or shUSF1, as determined by western blot analysis. (F) Representative blots. (G) Quantification for (F), n=5. *, $P<0.05$, vs CTL group.

that shEBNA2 and shUSF1 in LCL1 cells significantly decreased ATF4 protein levels compared to those in the CTL cells (**Figures 2F**, **2G**, S2B), suggesting that ATF4 expression was activated by EBNA2-mediated H3 demethylation and subsequently increased USF1 binding to the ATF4 promoter.

EBNA2 regulated lipid metabolism through ATF4 activation

Since ATF4 is a central regulator of cellular stress response, we investigated the effects of EBNA2 on lipid metabolism. LCL1 cells were infected with control (CTL), shEBNA2, shATF4, shUSF1, or shEBNA2 plus ATF4 expressing lentivirus (shEBNA2/↑ATF4). The efficient knockdown of gene expression by shRNA and ATF overexpression were confirmed by qPCR. We found that shEBNA2 reduced ATF4 mRNA level but had no effect on USF1 mRNA level, while shATF4 had no effect on the expression of USF1. Meanwhile, shUSF1 significantly reduced ATF4 levels (**Figure 3A**). We further examined ATF4 protein levels by western blot, and the results were consistent with the mRNA levels

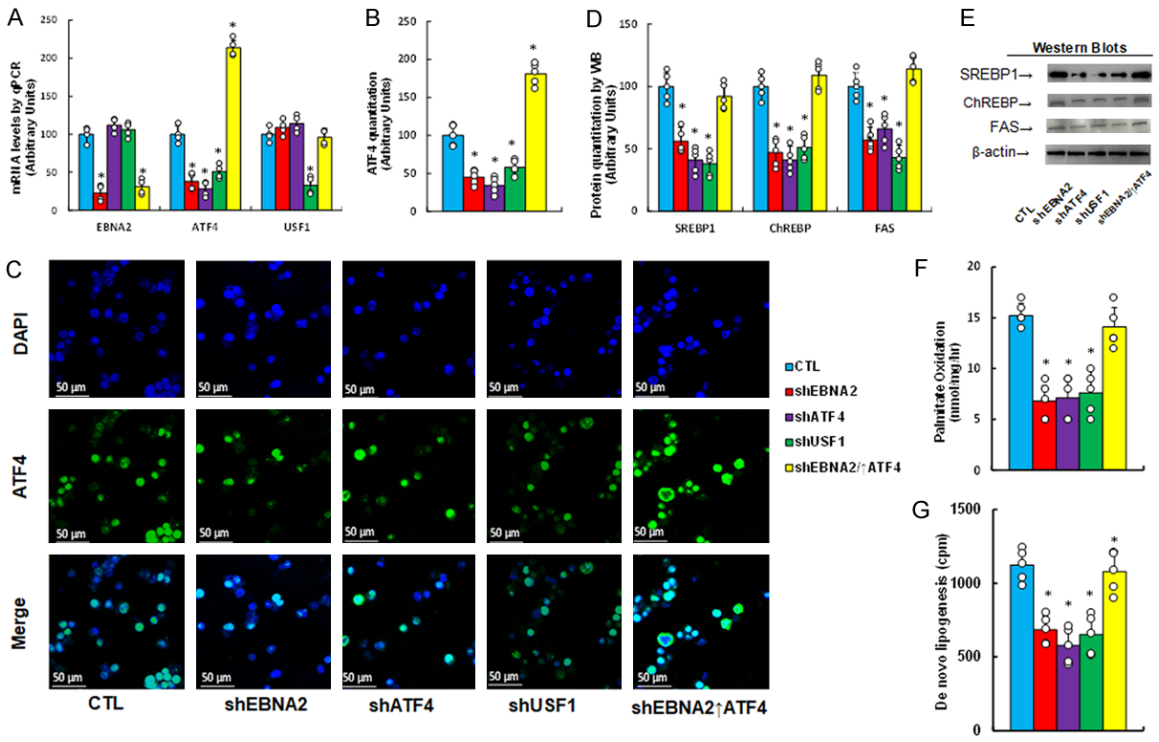

Figure 3. EBNA2 regulates lipid metabolism through ATF4 activation. LCL1 cells were infected with control (CTL), shEBNA2, shATF4, shUSF1 or shEBNA2 plus ATF4 expression (↑ATF4) lentivirus (shEBNA2/↑ATF4) and were examined. (A) mRNA level, n=4. (B) ATF4 quantitation, n=5. (C) Representative immunostaining (green) for ATF4 with nuclei staining by DAPI (blue) for (B). (D) Protein quantitation, n=5. (E) Representative western blots for (D). (F) Palmitate oxidation, n=5. (G) De novo lipogenesis, n=5. *, $P<0.05$, vs CTL group.

(**Figure 3B**, **3C**). We then determined the effect of these shRNAs on the expression of genes involved in lipid metabolism and found that treatment with shEBNA2, shATF4, and shUSF1 significantly reduced the protein levels of SREBP1, ChREBP, and FAS, but shEBNA2/↑ATF4 completely reversed the shEBNA2-induced effect (**Figures 3D**, **3E**, S2C). Consistently, treatment with shEBNA2, shATF4, and shUSF1 affected lipid metabolism in these cells as palmitate oxidation (**Figure 3F**) and de novo lipogenesis was significantly reduced (**Figure 3G**), while shEBNA2/↑ATF4 reversed this effect. Taken together, these results suggested that EBNA2 regulated lipid metabolism by activating the ATF4 pathway.

EBNA2 modulated redox balance and mitochondrial function through ATF4 activation

We also examined the effect of EBNA2 on redox balance and revealed that shEBNA2 treatment significantly increased both ROS (**Figure 4A**) and 8-oxo-dG generation (**Figure 4B**, **4C**). Treatment with shATF4 and shUSF1 partly, while shEBNA2/↑ATF4 completely reversed these effects. Furthermore, treatment with shEBNA2, shATF4, and shUSF1 significantly reduced mitochondrial replication (**Figure 4D**), ATP generation (**Figure 4E**), and mitochondrial membrane potential (ΔΨm, **Figure 4F**), but significantly increased the apoptosis rate (**Figure 4G**). In contrast, treatment with shEBNA2/↑ATF4 showed little effect (except for ATP generation) compared with the shEBNA2 group. Collectively, these results suggested that EBNA2 modulated redox balance and mitochondrial function partly through ATF4 activation.

EBNA2 regulated cell proliferation in vitro through ATF4 activation

The effect of EBNA2 expression on cell transformation and cell proliferation was investigated, and our results showed that shEBNA2 significantly reduced colony formation (**Figure 5A**, **5B**) and Ki-67 positive cell rate (**Figure 5C**, **5D**), compared with those in the CTL group, while

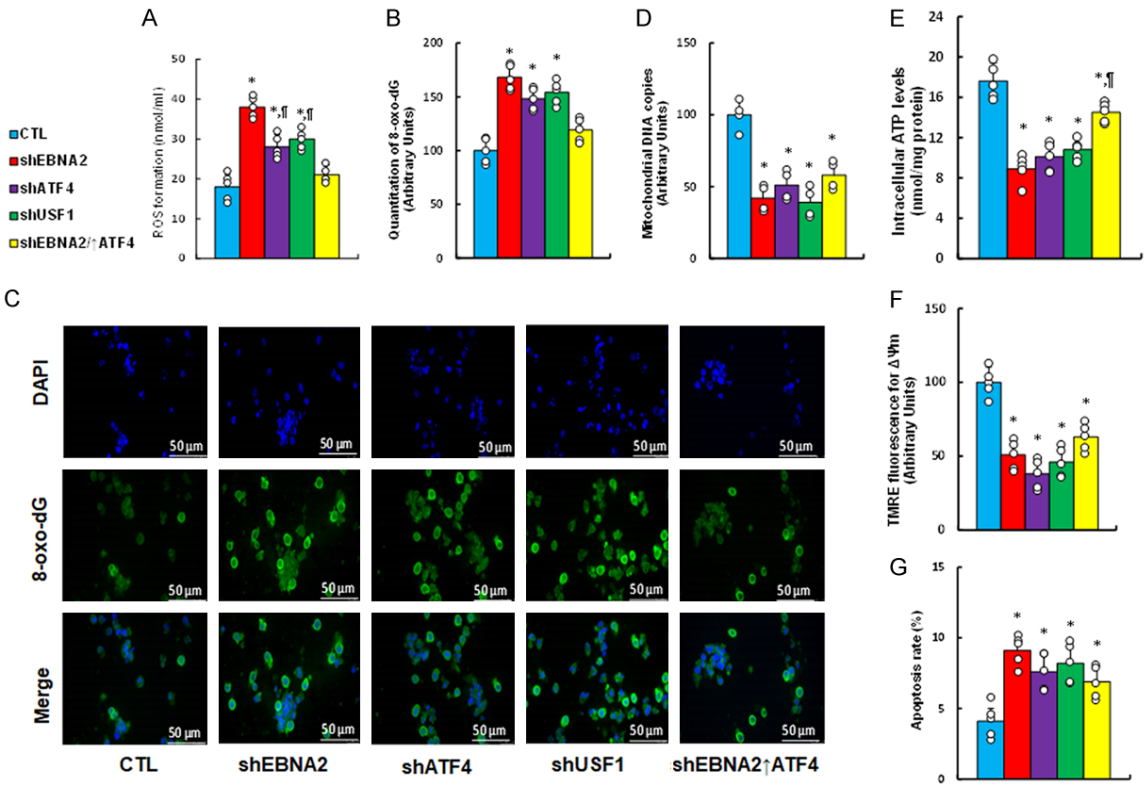

Figure 4. EBNA2 modulates redox balance and mitochondrial function through ATF4 activation. LCL1 cells were infected with control (CTL), shEBNA2, shATF4, shUSF1 or shEBNA2 plus ATF4 expression (↑ATF4) lentivirus (shEBNA2/↑ATF4) and examined. (A) ROS generation, n=5. (B) Quantitation of 8-oxo-dG staining, n=5. (C) Representative immunostaining (green) with nuclei staining by DAPI (blue) for (B). (D) Mitochondrial DNA copy number, n=4. (E) Intracellular ATP generation, n=5. (F) Mitochondrial membrane potential (ΔΨm), n=5. (G) Apoptosis, n=5. *, $P<0.05$, vs CTL group.

shATF4, shUSF1, and shEBNA2/↑ATF4 partly reversed this effect, suggesting that EBNA2 promoted cell proliferation partly through ATF4 activation.

EBNA2 regulated tumor growth in vivo through ATF4-mediated lipogenesis

More importantly, to confirm our in vitro cell line-based findings, we investigated the role of EBNA2 expression in tumor growth by using mouse xenograft tumor model. LCL1 cells were injected into mice through tail vein, and the tumor growth as well as the survival of the injected mice were monitored. We first measured the mRNA levels of EBNA2, shATF4, and shUSF1 in tumors and confirmed that shRNA lentivirus significantly knocked down the corresponding genes, while ATF4 lentivirus (↑ATF4) infection significantly increased ATF4 mRNA expression, indicating a successful lentivirus infection-mediated gene manipulation (**Figure 6A**). We then determined the expression of genes involved in lipid metabolism in tumors and found that treatment with shEBNA2, shATF4, and shUSF1 significantly reduced the protein levels of SREBP1, CHREBP, and FAS compared with the CTL group; shEBNA2/↑ATF4 treatment partly reversed this effect (**Figures 6B**, **6C**, S2D). In addition, the redox balance of tumor tissues was determined, and the data showed that shEBNA2 treatment significantly potentiated $O_2^{\cdot-}$ release compared with the CTL group and that treatment with shATF4, shUSF1 and shEBNA2/↑ATF4 ameliorated this effect (**Figure 6D**). When examining the tumor growth in lung, we found that shEBNA2 treatment significantly increased lung metastatic nodules (**Figure 6E**) and lung tumor spots (**Figure 6F**, **6G**) compared with the CTL group, and similarly, treatments with shATF4, shUSF1, and shEBNA2/↑ATF4 partly reversed this effect. Finally, mouse survival was evaluated, and the data indicated that shEBNA2 treatment signifi-

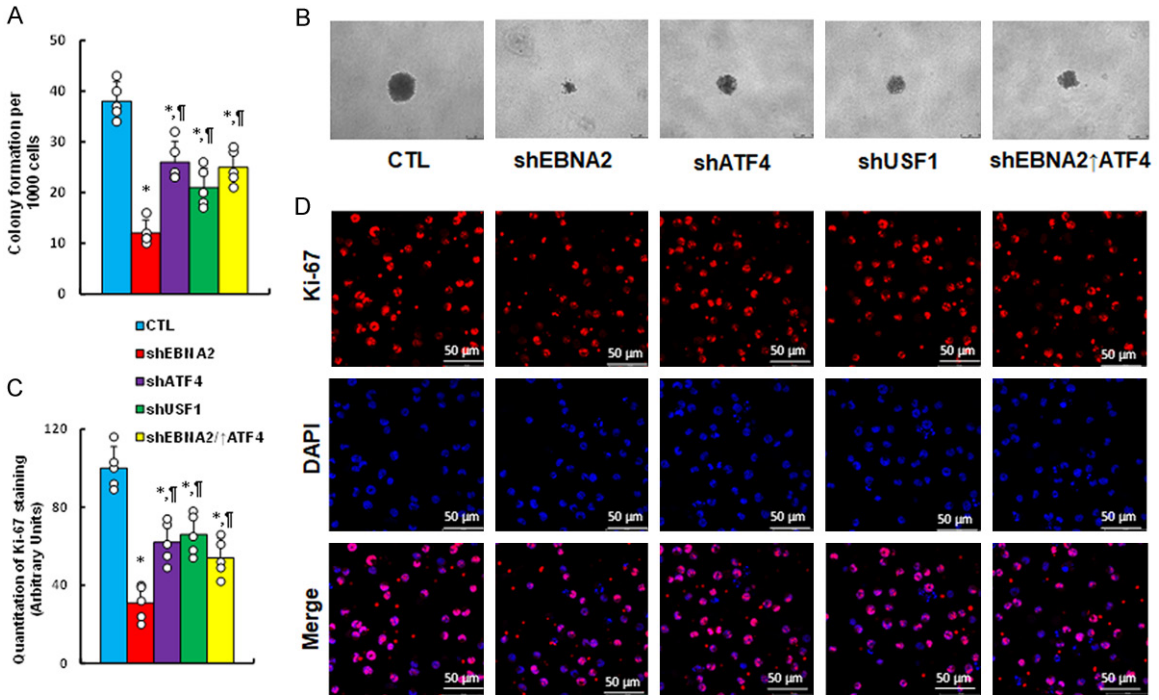

Figure 5. EBNA2 regulates cell proliferation *in vitro* through ATF4 activation. LCL1 cells were infected with control (CTL), shEBNA2, shATF4, shUSF1 or shEBNA2 plus ATF4 lentivirus (shEBNA2/↑ATF4) and examined. (A) Colony formation, n=5. (B) Representative images for (A). (C) Quantitation of Ki-67 staining, n=5. (D) Representative pictures for (C). *, $P<0.05$, vs CTL group; ¶, $P<0.05$, vs shEBNA2 group.

cantly increased mouse survival compared with the CTL group, whereas treatment with shATF4, shUSF1 and shEBNA2/↑ATF4 had smaller effects compared to shEBNA2 (**Figure 6H**). These results suggest that EBNA2 modulates tumor growth *in vivo* partly through ATF4 activation and the subsequently enhanced lipogenesis.

Schematic model for EBNA2-mediated ATF4 activation and tumorigenesis

Based on the results above, we proposed a working model for the mechanism underlying the regulation of ATF4 by EBNA2 and the subsequent increased tumorigenesis. In normal situations, ATF4 expression is suppressed by H3 methylation of the ATF4 promoter (**Figure 7A**); however, in the presence of EBV/EBNA2 exposure, ATF4 expression is upregulated by EBNA2-mediated demethylation of the ATF4 promoter (**Figure 7B**). ATF4 activation then modulates the expression of SREBP1, ChREBP, FAS, FAO, and lipogenesis (**Figure 7C**), and together with ATF4 activation-mediated modulation of oxidative stress and mitochondrial function, EBNA2-mediated ATF4 activation potentiates tumorigenesis (**Figure 7D**).

Discussion

In this study, we demonstrate that EBNA2 exposure causes persistent ATF4 expression and that ATF4 is regulated through EBNA2-mediated epigenetic changes, which subsequently increases the USF1 binding ability to the ATF4 promoter. Furthermore, EBNA2-mediated ATF4 activation modulates lipid metabolism and the expression of SREBP1, ChREBP and FAS, by which, together with ATF4-mediated redox balance and modulation of mitochondrial function, EBNA2 potentiates tumorigenesis through ATF4 activation.

Our findings are novel. First, we revealed that transient EBV/EBNA2 exposure induced persistent ATF4 expression through decreased H3K9me2 and H3K27me3 levels on the ATF4 promoter. In consistent with our findings, it has been reported that EBNA2 mediates epigenetic changes through DNA methylation [13], chromatin rearrangement [12] and phase separa-

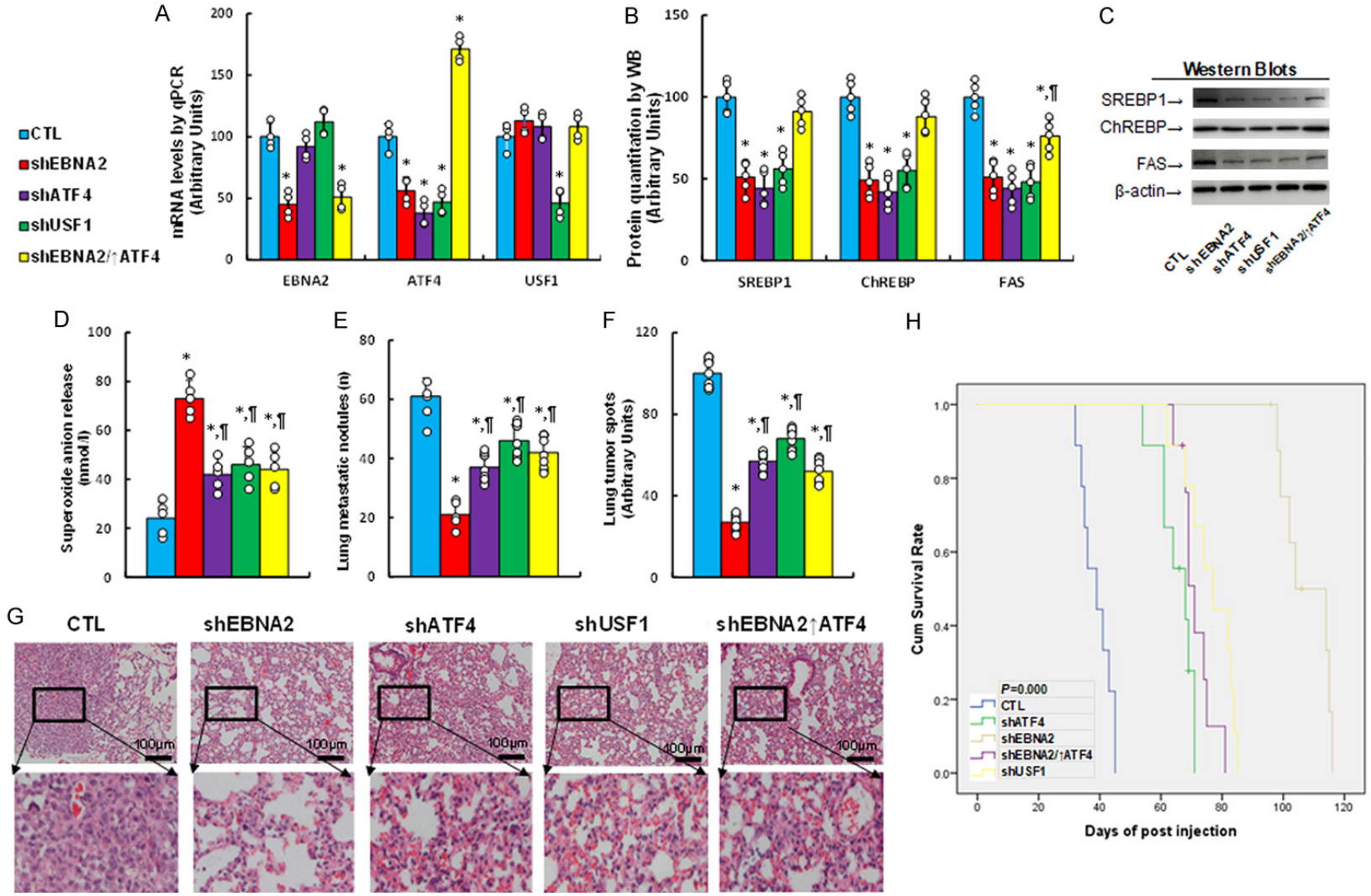

Figure 6. EBNA2 regulates tumor growth *in vivo* through ATF4-mediated effect. Treated LCL1 cells were injected through tail vein, and the tumor growth and the survival of mice were monitored. (A-C) Tumor tissues were isolated from the lung and analyzed. (A) mRNA levels, n=4. (B) Protein quantitation, n=5. (C) Representative western blots for (B). (D) Superoxide anion release from tissues, n=5. (E-G) Tumor colonies from lung were counted and used for H&E staining, n=9. (E) Metastatic nodules. (F) Quantitation of tumor spots. (G) Representative H&E staining for (F). (H) Kaplan-Meier analysis for mouse survival, *P* value represents log-rank Mantel-Cox test result, n=9. *, $P<0.05$, vs CTL group; ¶, $P<0.05$, vs shEBNA2 group.

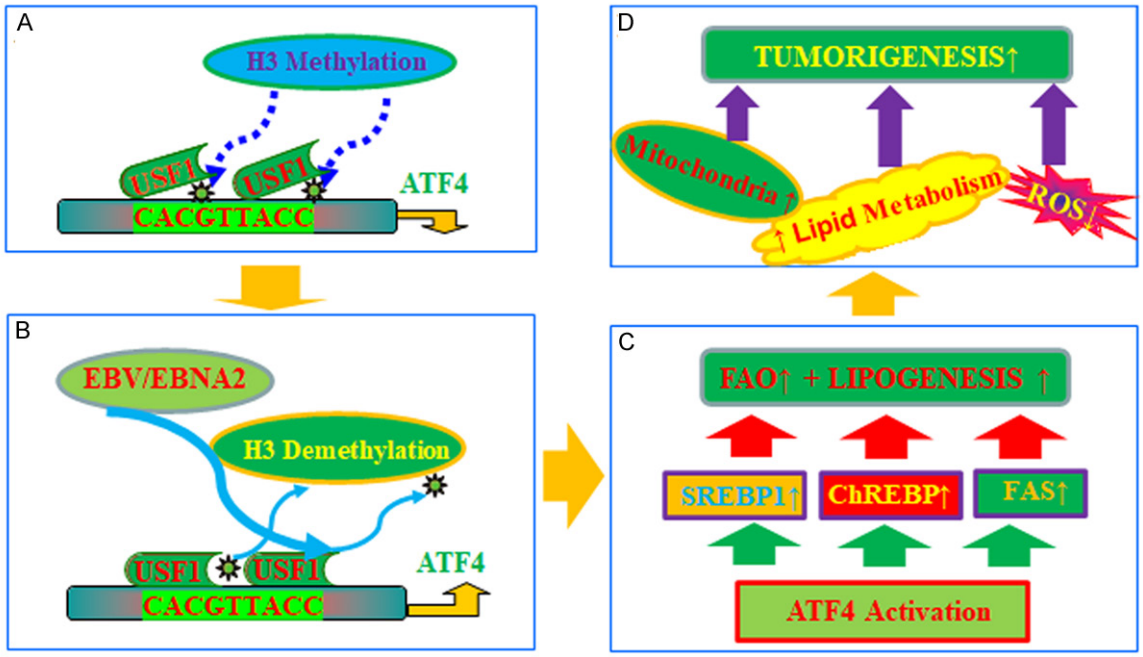

Figure 7. Schematic model for EBNA2-mediated ATF4 activation and tumorigenesis. A. ATF4 expression is suppressed by H3 methylation on the ATF4 promoter. B. ATF4 expression is up-regulated by EBNA2-mediated demethylation on the ATF4 promoter in the presence of EBV or EBNA2. C. ATF4 activation modulates the expression of SREBP1, ChREBP and FAS as well as FAO and lipogenesis. D. ATF4 activation-mediated modulation of lipid metabolism, and ROS generation and mitochondrial function promotes tumorigenesis. Abbreviations: ATF4: activates transcription factor-4; ChREBP: carbohydrate-responsive element-binding protein; EBNA2: Epstein-Barr virus nuclear antigen 2; EBV: Epstein-Barr virus; FAS: fatty acid synthase; FAO: fatty acid oxidation; H3: histone 3; ROS: reactive oxygen species; SREBP1: sterol regulatory element-binding protein 1; USF1: upstream stimulating factor 1.

tion [10], indicating that EBNA2 expression triggers epigenetic changes. Nevertheless, whether the epigenetic modifications on the ATF4 promoter is a direct effect of EBNA2 needs further investigation. EBNA2-mediated epigenetic changes and persistent gene regulation of ATF4 may play important roles in cell transformation and tumorigenesis [6]. Although ATF4 activation is usually regulated at the translational level due to the phosphorylation of eIF2α as part of the integrated stress response [40], our study showed ATF4 regulation at the transcriptional level by epigenetic changes, indicating that EBNA2-mediated gene expression is relatively persistent, which is favorable for tumorigenesis. Interestingly, our study demonstrated that EBNA2-mediated epigenetic changes increased USF1 binding to the ATF4 promoter and subsequently activated ATF4 expression. Furthermore, EBNA2 expression increased USF1 binding to the ATF4 promoter with ATF4 upregulation, whereas USF1 knockdown suppressed ATF4 expression. Hence, our data indicated that EBNA2 regulated ATF4 activation and lipid metabolism through USF1, which subsequently modulated lipogenesis via SREBP1, ChREBP, and FAS [34, 41, 42].

Our data also showed that ATF4 activation increased the expression of SREBP1, ChREBP, and FAS as well as potentiated FAO and lipogenesis, while ATF4 knockdown suppressed the gene expression and lipid metabolism, indicating that ATF4 may modulate lipid metabolism [27, 43]. It has been reported that ATF4 does not directly upregulate mitochondrial FAO but may modulate mitochondrial function and upregulate antioxidant machinery to mitigate the presence of defective mitochondria [44, 45]. As a transcription factor, ATF4 may regulate the expression of SREBP1, ChREBP, and FAS either directly or indirectly and subsequently modulate lipid metabolism, although the mechanism remains unclear.

Moreover, we observed that knockdown of either EBNA2 or ATF4 increased oxidative

stress, while ATF4 overexpression partly reverses this effect, indicating that ATF4 is involved in the redox balance in tumor cells [17, 24]. In addition, knockdown of either EBNA2 or ATF4 modulated mitochondrial function [25], including decreased mitochondrial DNA copies, intracellular ATP formation, ΔΨm, and potentiated apoptosis rate, indicating that EBNA2-mediated ATF4 activation plays an important role in sustaining mitochondrial function in tumor cells. It has been proposed that ATF4 may modulate redox balance and mitochondrial function through mitochondrial fat oxidation and lipogenesis [26, 27, 46]. In this study, we showed that ATF4 overexpression could rescue ROS generation, mitochondrial function, and lipid metabolism in the absence of EBNA2, and EBNA2 triggers this effect in an ATF4-dependent manner, indicating that EBNA2 transient exposure may cause persistent changes during tumorigenesis, which can explain why many forms of lymphoma show the absence of EBV.

More significantly, using in vivo mouse model, we confirmed that EBNA2-mediated ATF4 activation increased the gene expression of SREBP1, ChREBP, and FAS [16], subsequently potentiating FAO and lipogenesis as well as modulating redox balance and mitochondrial function. In addition, knockdown of EBNA2/ATF4 significantly increased mouse survival in the *in vivo* mouse model. Therefore, we speculate that the major function of ATF4 in promoting tumorigenesis is to increase the antioxidant activity and regulate ROS production; however, the precise mechanisms of ATF4 function remain to be fully elucidated [44, 45]. Although our data suggest that EBNA2 mediates tumorigenesis through ATF4 activation and altered lipid metabolism [19], EBNA2 may also contribute to tumorigenesis through other pathways, such as Myc activation, Notch signaling, and PD-L1 expression [6-8, 28].

Conclusions

In summary, EBNA2 expression causes persistent ATF4 activation through EBNA2-mediated epigenetic changes and enhances USF1 binding to the ATF4 promoter. Furthermore, EBNA2-mediated ATF4 activation increases the expression of SREBP1, ChREBP, and FAS, as well as modulates lipid metabolism, redox balance, and mitochondrial function, which subsequently contributes to tumorigenesis. Given our findings that EBNA2 mediates tumorigenesis through ATF4 activation and modulation of lipid metabolism, our study may reveal novel potential targets for the clinical treatment of EBV-mediated tumors.

Acknowledgements

EBNA2 shRNA lentivirus, EBNA2 adenovirus, and related empty controls were kindly provided by Dr. Haimou Zhang (Hubei University, China). This study was financially supported by the Shenzhen Science and Technology Innovation Project #: JCYJ20210324105802007; Shenzhen Health System Research Project #: SZXJ2018081; Research Foundation of Peking University Shenzhen Hospital Project #: JCYJ2020017; and National Natural Science Foundation of China, Project #: 82170191 & 82100210.

The protocols for animal (#2021-092) and human subjects (#2020-050) were approved by the Peking University Shenzhen Hospital Ethical Committee and written consent was obtained from all participants.

Disclosure of conflict of interest

None.

Abbreviations

ATF4, activating transcription factor-4; ChREBP, carbohydrate-responsive element-binding protein; EBNA2, Epstein-Barr virus nuclear antigen 2; EBV, Epstein-Barr virus; FAS, fatty acid synthase; MMP, mitochondrial membrane potential (ΔΨm); SREBP1, sterol regulatory element-binding protein 1; USF1, upstream stimulating factor 1.

Address correspondence to: Drs. Paul Yao and Hongyu Zhang, Department of Hematology, Peking University Shenzhen Hospital, Shenzhen 518036, Guangdong, P. R. China. Tel: +86-13049687987; E-mail: vasilis112@yahoo.com (PY); Tel: +86-13510331595; E-mail: zyiqu@163.com (HYZ)

References

[1] Zhu J, Li L, Tong J, Hui C, Wong CH, Lo KW, Chan R, Ai QY, Hui EP, Chan AT, To KF, Tao Q and Ma BB. Targeting the polycomb repressive complex-2 related proteins with novel combi-

national strategies for nasopharyngeal carcinoma. Am J Cancer Res 2020; 10: 3267-3284.
[2] Liu GY, Li WZ, Xie CB, Liang H, Xia WX and Xiang YQ. Trajectories of EBV DNA and identifying the potential long-term survivors in metastatic nasopharyngeal carcinoma. Am J Cancer Res 2021; 11: 3946-3955.
[3] Ayoubian H, Frohlich T, Pogodski D, Flatley A, Kremmer E, Schepers A, Feederle R, Arnold GJ and Grasser FA. Antibodies against the monomethylated arginine-glycine repeat (MMA-RG) of the Epstein-Barr virus nuclear antigen 2 (EBNA2) identify potential cellular proteins targeted in viral transformation. J Gen Virol 2017; 98: 2128-2142.
[4] Chou YC, Lin SJ, Lu J, Yeh TH, Chen CL, Weng PL, Lin JH, Yao M and Tsai CH. Requirement for LMP1-induced RON receptor tyrosine kinase in Epstein-Barr virus-mediated B-cell proliferation. Blood 2011; 118: 1340-1349.
[5] Wang LW, Jiang S and Gewurz BE. Epstein-barr virus LMP1-mediated oncogenicity. J Virol 2017; 91: e01718-16.
[6] Golden S, Yu XM, Odorico S, Jain V, Marin A, Ma S, Kenney S and Chen H. The Epstein-Barr virus EBNA2 protein induces a subset of NOTCH target genes in thyroid cancer cell lines but fails to suppress proliferation. Surgery 2017; 161: 195-201.
[7] Anastasiadou E, Stroopinsky D, Alimperti S, Jiao AL, Pyzer AR, Cippitelli C, Pepe G, Severa M, Rosenblatt J, Etna MP, Rieger S, Kempkes B, Coccia EM, Sui SJH, Chen CS, Uccini S, Avigan D, Faggioni A, Trivedi P and Slack FJ. Epstein-Barr virus-encoded EBNA2 alters immune checkpoint PD-L1 expression by downregulating miR-34a in B-cell lymphomas. Leukemia 2019; 33: 132-147.
[8] Muhe J and Wang F. Species-specific functions of Epstein-Barr virus nuclear antigen 2 (EBNA2) reveal dual roles for initiation and maintenance of B cell immortalization. PLoS Pathog 2017; 13: e1006772.
[9] Zhang X, Schuhmachers P, Mourao A, Giansanti P, Murer A, Thumann S, Kuklik-Roos C, Beer S, Hauck SM, Hammerschmidt W, Kuppers R, Kuster B, Raab M, Strebhardt K, Sattler M, Munz C and Kempkes B. PLK1-dependent phosphorylation restrains EBNA2 activity and lymphomagenesis in EBV-infected mice. EMBO Rep 2021; 22: e53007.
[10] Peng Q, Wang L, Wang J, Liu C, Zheng X, Zhang X, Wei L, Li Z, Wu Y, Wen Y, Cao P, Liao Q, Yan Q and Ma J. Epstein-Barr virus EBNA2 phase separation regulates cancer-associated alternative RNA splicing patterns. Clin Transl Med 2021; 11: e504.
[11] Li Z, Zhou Z, Wu X, Zhou Q, Liao C, Liu Y, Li D, Shen L, Feng D and Yang L. LMP1 promotes nasopharyngeal carcinoma metastasis through NTRK2-mediated anoikis resistance. Am J Cancer Res 2020; 10: 2083-2099.
[12] Yang Y, Ye X, Dai R, Li Z, Zhang Y, Xue W, Zhu Y, Feng D, Qin L, Wang X, Lei B, Liao S and Hao B. Phase separation of Epstein-Barr virus EBNA2 protein reorganizes chromatin topology for epigenetic regulation. Commun Biol 2021; 4: 967.
[13] Lu F, Wiedmer A, Martin KA, Wickramasinghe PJMS, Kossenkov AV and Lieberman PM. Coordinate regulation of TET2 and EBNA2 controls the DNA methylation state of latent epstein-barr virus. J Virol 2017; 91: e00804-17.
[14] Glaser LV, Rieger S, Thumann S, Beer S, Kuklik-Roos C, Martin DE, Maier KC, Harth-Hertle ML, Gruning B, Backofen R, Krebs S, Blum H, Zimmer R, Erhard F and Kempkes B. EBF1 binds to EBNA2 and promotes the assembly of EBNA2 chromatin complexes in B cells. PLoS Pathog 2017; 13: e1006664.
[15] Ponnusamy R, Khatri R, Correia PB, Wood CD, Mancini EJ, Farrell PJ and West MJ. Increased association between Epstein-Barr virus EBNA2 from type 2 strains and the transcriptional repressor BS69 restricts EBNA2 activity. PLoS Pathog 2019; 15: e1007458.
[16] Piccaluga PP, Weber A, Ambrosio MR, Ahmed Y and Leoncini L. Epstein-Barr virus-induced metabolic rearrangements in human B-cell lymphomas. Front Microbiol 2018; 9: 1233.
[17] Wortel IMN, van der Meer LT, Kilberg MS and van Leeuwen FN. Surviving stress: modulation of ATF4-mediated stress responses in normal and malignant cells. Trends Endocrinol Metab 2017; 28: 794-806.
[18] Bai X, Ni J, Beretov J, Wasinger VC, Wang S, Zhu Y, Graham P and Li Y. Activation of the eIF2alpha/ATF4 axis drives triple-negative breast cancer radioresistance by promoting glutathione biosynthesis. Redox Biol 2021; 43: 101993.
[19] Wu TS, Tan CT, Chang CC, Lin BR, Lai WT, Chen ST, Kuo MY, Rau CL, Jaw FS and Chang HH. B-cell lymphoma/leukemia 10 promotes oral cancer progression through STAT1/ATF4/S100P signaling pathway. Oncogene 2015; 34: 1207-1219.
[20] Wang M, Lu Y, Wang H, Wu Y, Xu X and Li Y. High ATF4 expression is associated with poor prognosis, amino acid metabolism, and autophagy in gastric cancer. Front Oncol 2021; 11: 740120.
[21] Yu Y, Liu B, Li X, Lu D, Yang L, Chen L, Li Y, Cheng L, Lv F, Zhang P, Song Y and Xing Y. ATF4/CEMIP/PKCalpha promotes anoikis resistance by enhancing protective autophagy in prostate cancer cells. Cell Death Dis 2022; 13: 46.

[22] Yu XX, Zhu MY, Wang JR, Li H, Hu P, Qing YJ, Wang XY, Wang HZ, Wang ZY, Xu JY, Guo QL and Hui H. LW-213 induces cell apoptosis in human cutaneous T-cell lymphomas by activating PERK-eIF2alpha-ATF4-CHOP axis. Acta Pharmacol Sin 2021; 42: 290-300.

[23] Torrence ME, MacArthur MR, Hosios AM, Valvezan AJ, Asara JM, Mitchell JR and Manning BD. The mTORC1-mediated activation of ATF4 promotes protein and glutathione synthesis downstream of growth signals. Elife 2021; 10: e63326.

[24] Szewczyk MM, Luciani GM, Vu V, Murison A, Dilworth D, Barghout SH, Lupien M, Arrowsmith CH, Minden MD and Barsyte-Lovejoy D. PRMT5 regulates ATF4 transcript splicing and oxidative stress response. Redox Biol 2022; 51: 102282.

[25] Krall AS, Mullen PJ, Surjono F, Momcilovic M, Schmid EW, Halbrook CJ, Thambundit A, Mittelman SD, Lyssiotis CA, Shackelford DB, Knott SRV and Christofk HR. Asparagine couples mitochondrial respiration to ATF4 activity and tumor growth. Cell Metab 2021; 33: 1013-1026, e6.

[26] De Oliveira MP and Liesa M. The role of mitochondrial fat oxidation in cancer cell proliferation and survival. Cells 2020; 9: 2600.

[27] Ren LP, Yu X, Song GY, Zhang P, Sun LN, Chen SC, Hu ZJ and Zhang XM. Impact of activating transcription factor 4 signaling on lipogenesis in HepG2 cells. Mol Med Rep 2016; 14: 1649-1658.

[28] Burton EM and Gewurz BE. Epstein-Barr virus oncoprotein-driven B cell metabolism remodeling. PLoS Pathog 2022; 18: e1010254.

[29] Hulse M, Johnson SM, Boyle S, Caruso LB and Tempera I. Epstein-Barr virus-encoded latent membrane protein 1 and B-cell growth transformation induce lipogenesis through fatty acid synthase. J Virol 2021; 95: e01857-20.

[30] Lo AK, Lung RW, Dawson CW, Young LS, Ko CW, Yeung WW, Kang W, To KF and Lo KW. Activation of sterol regulatory element-binding protein 1 (SREBP1)-mediated lipogenesis by the Epstein-Barr virus-encoded latent membrane protein 1 (LMP1) promotes cell proliferation and progression of nasopharyngeal carcinoma. J Pathol 2018; 246: 180-190.

[31] Zheng S, Matskova L, Zhou X, Xiao X, Huang G, Zhang Z and Ernberg I. Downregulation of adipose triglyceride lipase by EB viral-encoded LMP2A links lipid accumulation to increased migration in nasopharyngeal carcinoma. Mol Oncol 2020; 14: 3234-3252.

[32] Wang LW, Wang Z, Ersing I, Nobre L, Guo R, Jiang S, Trudeau S, Zhao B, Weekes MP and Gewurz BE. Epstein-Barr virus subverts mevalonate and fatty acid pathways to promote infected B-cell proliferation and survival. PLoS Pathog 2019; 15: e1008030.

[33] Wei C, Wang P, Dong Q, Ma XH, Lu M, Qi S, Shi JH, Xie Z, Ren AJ and Zhang WJ. ChREBP-regulated lipogenesis is not required for the thermogenesis of brown adipose tissue. Int J Obes (Lond) 2022; 46: 1068-1075.

[34] Wang Y, Viscarra J, Kim SJ and Sul HS. Transcriptional regulation of hepatic lipogenesis. Nat Rev Mol Cell Biol 2015; 16: 678-689.

[35] Yu H, Zhang H, Chu Z, Ruan Q, Chen X, Kong D, Huang X, Li H, Tang H, Wu H, Wang Y, Xie W, Ding Y and Yao P. Combination of betulinic acid and chidamide synergistically inhibits Epstein-Barr virus replication through over-generation of reactive oxygen species. Oncotarget 2017; 8: 61646-61661.

[36] Hui KF and Chiang AK. Suberoylanilide hydroxamic acid induces viral lytic cycle in Epstein-Barr virus-positive epithelial malignancies and mediates enhanced cell death. Int J Cancer 2010; 126: 2479-2489.

[37] Li H, Liu Z, Gou Y, Yu H, Siminelakis S, Wang S, Kong D, Zhou Y, Liu Z, Ding Y and Yao D. Estradiol mediates vasculoprotection via ERRα-dependent regulation of lipid and ROS metabolism in the endothelium. J Mol Cell Cardiol 2015; 87: 92-101.

[38] Yao D, Shi W, Gou Y, Zhou X, Yee Aw T, Zhou Y and Liu Z. Fatty acid-mediated intracellular iron translocation: a synergistic mechanism of oxidative injury. Free Radic Biol Med 2005; 39: 1385-1398.

[39] Akie TE and Cooper MP. Determination of fatty acid oxidation and lipogenesis in mouse primary hepatocytes. J Vis Exp 2015; e52982.

[40] Andrysik Z, Sullivan KD, Kieft JS and Espinosa JM. PPM1D suppresses p53-dependent transactivation and cell death by inhibiting the integrated stress response. Nat Commun 2022; 13: 7400.

[41] Kersten S. Mechanisms of nutritional and hormonal regulation of lipogenesis. EMBO Rep 2001; 2: 282-286.

[42] Viscarra J and Sul HS. Epigenetic regulation of hepatic lipogenesis: role in hepatosteatosis and diabetes. Diabetes 2020; 69: 525-531.

[43] Chen L, Liu X, Zhou H, Li G, Huang F, Zhang J, Xia T, Lei W, Zhao J, Li C and Chen M. Activating transcription factor 4 regulates angiogenesis under lipid overload via methionine adenosyltransferase 2A-mediated endothelial epigenetic alteration. FASEB J 2021; 35: e21612.

[44] Guo X, Aviles G, Liu Y, Tian R, Unger BA, Lin YT, Wiita AP, Xu K, Correia MA and Kampmann M. Mitochondrial stress is relayed to the cytosol by an OMA1-DELE1-HRI pathway. Nature 2020; 579: 427-432.

[45] Hunt RJ, Granat L, McElroy GS, Ranganathan R, Chandel NS and Bateman JM. Mitochondrial stress causes neuronal dysfunction via an ATF4-dependent increase in L-2-hydroxyglutarate. J Cell Biol 2019; 218: 4007-4016.

[46] Chen JJ and Zhang S. Translational control by heme-regulated eIF2alpha kinase during erythropoiesis. Curr Opin Hematol 2022; 29: 103-111.

Supplementary Materials

Materials and methods

Reagents and materials

Written consent was obtained from participants and peripheral blood mononuclear cells (PBMC) from healthy patients were isolated from peripheral blood using Lymphoprep™ reagents (#07861). Human B lymphocytes (HBL) were isolated from healthy PBMC cells using EasySep™ Human B Cell Isolation Kit (#17954). Some of healthy B lymphocytes were conditionally immortalized using hTERT lentivirus vector with an extended life span to achieve a higher transfection efficiency and experimental stability [1, 2], or they were transformed by EBV virus infection to obtain lymphoblastoid cell line 1 (LCL1) as described previously in our lab [3]. Tumor cell lines B95-8 (CVCL_1953) and Namalwa (CVCL_0067) were purchased from ATCC and cultured in RPMI 1640 medium containing 2 mmol/l glutamine supplemented with 100 U/ml penicillin, 100 μg/ml streptomycin, 10% human serum and 1000 U/ml recombinant human IL-2. The B95-8 cell line was used for EBV viral production and subsequent concentration for the infection of human B lymphocytes according to the previous protocol [4]. The Namalwa cell line was used for the detection of EBV copy number. All cells were maintained in a humidified incubator with 5% CO_2 at 37°C. All the cell lines were authenticated in the past three years and they were derived from the correct species and donor, and contamination-free, and all experiments were performed with mycoplasma-free cells.

Cell line authentication process. Cell lines were cultured and harvested, and the genomic DNA was extracted from cells using a QIAamp DNA Mini Kit (Qiagen). DNA concentration was determined by NanoDrop 2000c system, and DNA was amplified by ABI9700 PCR System, the electrophoresis and fragment isolation were conducted by ABI3 730XL system, and gene analysis was conducted by software GeneMapper® ID-X 1.5. Human cell lines (Namalwa and LCL1) were submitted for STR (Short Tandem Repeat) Identification, while B95-8 cell line was submitted for Species Identification, which conducted by Applied Biosystems, China. The cell line was identified to be acceptable when it had >80% matching with US National Standard ASN-0002-2011.

Antibodies for ATF4 (sc-390063), β-actin (sc-47778), ChREBP (sc-515922), FAS (sc-48357), Ki-67 (sc-101861), Smad4 (sc-7966), Sp1 (sc-17824), SREBP1 (sc-13551), USF1 (sc-390027), Zic3 (sc-101201) were obtained from Santa Cruz Biotechnology. Antibodies for H3K9me2 (ab1220), H3K9me3 (ab8898), H3K27me2 (ab24684), H3K27me3 (ab6002), EBNA2 (ab90543), HNF3 (ab108422) and SPZ1 (ab235302) were obtained from Abcam. The EBNA2 adenovirus and related empty control for EBNA2 transient infection as well as shEBNA2 lentivirus were kindly provided by Dr. Haimou Zhang from Hubei University. The antibody for 8-oxo-dG (4354-MC-050) was obtained from Novus Biologicals.

Construction of human ATF4 reporter plasmid

In order to construct ATF4 reporter plasmids, the ATF4 gene promoter (2 kb upstream of the transcription start site plus first exon) was amplified from Ensembl gene ID: ENST00000337304.2 ATF4-201 (for ATF4) by PCR from human genomic DNA and subcloned into the pGL3-basic vector (#E1751, Promega) using the restriction sites of KpnI and Bgl II with the following primers: ATF4 forward: 5'-gcgc-ggtacc-ggg ctc aag caa tcc tcc cac-3' (KpnI) and ATF4 reverse: 5'-atcg-agatct-cct tgc tgt tgt tgg agg gac-3' (Bgl II). In order to map ATF4 promoter activity, the related deletion promoter constructs were generated by PCR methods and subcloned into the pGL3-basic vector.

Preparation of ATF4/USF1 expression lentivirus

The cDNA for human ATF4 and USF1 (obtained from Open Biosystems) was subcloned into the pLVX-Puro vector (from Clontech) with the restriction sites of EcoR1 and BamH1 using the following primers: ATF4 forward primer: 5'-gtac-gaattc (EcoR1) - agc cat ttc tac ttt gcc cgc-3' and ATF4 reverse primer:

5'-gtac-ggatcc (BamH1) - ttt ttt ttt ttt ttt act ttc cct aca-3'; USF1 forward primer: 5'-gtac-gaattc (EcoR1) - gcc cct cac caa cat ggc cgc-3' and USF1 reverse primer: 5'-gtac-ggatcc (BamH1) - aga taa aat tgt tca aag cca-3'. The lentivirus for either ATF4, USF1 or empty control (CTL) was expressed through Lenti-X™ Lentiviral Expression Systems (from Clontech) per manufacturers' instructions.

Preparation of gene knockdown lentivirus

The shRNA lentivirus particles for human ATF4 (sc-35112-V), USF1 (sc-36783-V) or non-target control (sc-108080) were obtained from Santa Cruz Biotech, and the shRNA lentivirus for EBNA2 was obtained from Dr. Haimou Zhang (Hubei University, China); these lentiviruses were used for infection of LCL1 cells. The positive knockdown cells were selected using 10 μg/ml of puromycin and the stable knockdown cell line was confirmed by real time PCR based on an mRNA decrease of more than 65% compared to the control group (see primers in Table S1).

RT reaction and real-time quantitative PCR

Total RNA from treated cells was extracted using the RNeasy Micro Kit (Qiagen), and the RNA was reverse transcribed using an Omniscript RT kit (Qiagen). All the primers were designed using Primer 3 Plus software with the Tm at 60°C, primer size of 21 bp, and product length in the range of 140-160 bp (see Table S1). The primers were validated with an amplification efficiency in the range of 1.9-2.1 and the amplified products were confirmed with agarose gel. Real-time quantitative PCR was run on iCycler iQ (Bio-Rad) using the Quantitect SYBR green PCR kit (Qiagen). The PCR was performed by denaturing at 95°C for 8 min followed by 45 cycles of denaturation at 95°C, annealing at 60°C, and extension at 72°C for 10 s, respectively. 1 μl of each cDNA was used to measure target genes. β-actin was used as the housekeeping gene for transcript normalization, and the mean values were used to calculate relative transcript levels with the ΔΔCT method per instructions from Qiagen. In brief, the amplified transcripts were quantified by the comparative threshold cycle method using β-actin as a normalizer. Fold changes in gene mRNA expression were calculated as $2^{-\Delta\Delta CT}$ with CT = threshold cycle, ΔCT = CT (target gene) - CT (β-actin), and the ΔΔCT = ΔCT (experimental) - ΔCT (reference).

Luciferase reporter assay

1.0×10^5 of cells were seeded in a 6-well plate with complete medium to grow until they reached 80% confluence. Cells were then co-transfected using 3 μg of reporter constructs, together with 0.2 μg of pRL-CMV-Luc *Renilla* plasmid (from Promega). The treated cells were then harvested and the luciferase activity assays were carried out using the Dual-Luciferase™ Assay System (Promega). The transfection efficiencies were normalized using a co-transfected *Renilla* plasmid according to manufacturers' instructions and the reporter activities for PGC1β and OGG1 were calculated.

Chromatin immunoprecipitation (ChIP)

Cells were washed and crosslinked using 1% formaldehyde for 20 min and terminated by 0.1 M glycine. Cell lysates were sonicated and centrifuged. 500 μg of protein were pre-cleared by BSA/salmon sperm DNA with preimmune IgG and a slurry of Protein A Agarose beads. Immunoprecipitations were performed with the indicated antibodies, BSA/salmon sperm DNA and a 50% slurry of Protein A agarose beads. Input and immunoprecipitates were washed and eluted before then being incubated with 0.2 mg/ml Proteinase K for 2 h at 42°C, followed by 6 h at 65°C to reverse the formaldehyde crosslinking. DNA fragments were recovered through phenol/chloroform extraction and ethanol precipitation. A ~150 bp fragment on the related promoter was amplified by real-time PCR (qPCR) using the primers provided in Table S1.

Western blotting

Cells were lysed in an ice-cold lysis buffer (0.137 M NaCl, 2 mM EDTA, 10% glycerol, 1% NP-40, 20 mM Tris base, pH 8.0) with protease inhibitor cocktail (Sigma). The proteins were separated in 10% SDS-PAGE and transferred to the PVDF membrane, which was then blotted using primary antibodies (1:1000)

and then simultaneously incubated with the differentially labeled species-specific secondary antibodies, anti-RABBIT IRDye™ 800CW (green) and anti-MOUSE (or goat) ALEXA680 (red). Membranes were scanned and quantitated using the ODYSSEY Infrared Imaging System (LI-COR, NE) [5].

Immunostaining

The treated LCL1 cells were transferred to cover slips coated with 0.1% gelatin, fixed by 3.7% formaldehyde at 37°C for 15 min, permeabilized by 1% BSA + 0.2% Triton X-100 in PBS for 1 hour, and then blotted with 40 μg/ml (dilute 1:50) of related antibody for either 8-oxo-dG or Ki-67 for 2 hours. The cells were then washed three times and the FITC/Texas Red labeled anti-mouse/rabbit secondary antibody (1:100) was added for blotting for another 1 hour. After thorough washing, the slides were visualized and photographed; cell nuclei were stained with 4',6-diamidino-2-phenylindole dihydrochloride (DAPI, #D9542, from Sigma) and the staining was quantitated by Image J.

Measurement of oxidative stress

Treated cells were seeded in a 96-well plate and incubated with 10 μM CM-H2DCFDA (Invitrogen) for 45 min at 37°C. Then, the intracellular formation of reactive oxygen species was measured at excitation/emission wavelengths of 485/530 nm using a FLx800 microplate fluorescence reader (Bio-Tek), and the data was normalized as arbitrary units [6].

Measurement of mitochondrial function

Mitochondrial DNA copies: Genomic DNA was extracted from treated MM.1R cells using a QIAamp DNA Mini Kit (Qiagen) and the mitochondrial DNA was extracted using the REPLI-g Mitochondrial DNA Kit (Qiagen). The purified DNA was used for the analysis of genomic β-actin (marker of the nuclear gene) and ATP6 (ATP synthase F0 subunit 6, marker of the mitochondrial gene) respectively using the qPCR method as mentioned above. The primers for genomic β-actin are as follows: forward 5'-ctg gac ttc gag caa gag atg-3' and reverse: 5'-agg aag gaa ggc tgg aag agt-3'. Primers for ATP6: forward 5'-cat tta cac caa cca ccc aac-3' and reverse 5'-tat ggg gat aag ggg tgt agg-3'. The mitochondrial DNA copies were obtained from relative ATP6 copies that were normalized by β-actin copies using the $^{\Delta\Delta}$CT method [6-8].

Intracellular ATP level: The intracellular ATP level was determined using the luciferin/luciferase-induced bioluminescence system. An ATP standard curve was generated at concentrations of 10^{-12}-10^{-3} M. Intracellular ATP levels were calculated and expressed as nmol/mg protein [6-8].

Mitochondria membrane potential: Mitochondrial membrane potential (MMP, Δψm) was measured using TMRE (from Molecular Probes T-669) staining. A 600 μM T-669 stock solution was prepared using DMSO. Cells were grown on coverslips and immersed in 600 nM TMRE for 20 min at 37°C to load them with dye. The labeling medium was then aspirated and the cells were immersed in 150 nM TMRE to maintain the equilibrium distribution of the fluorophore. The coverslips were mounted with live cells onto confocal microscopes to image the cells using 548 nm excitation/573 nm emission filters. The intensity of TMRE fluorescence was measured using Image J software. Data from 10-20 cells were collected for each experimental condition and mean values of fluorescence intensity ± SEM were calculated [8, 9].

Measurement of apoptosis: Apoptosis was evaluated by TUNEL assay using the In Situ Cell Death Detection Kit™ (Roche). Cells were fixed in 4% paraformaldehyde and labeled by TUNEL reagents. Stained cells were photographed by a fluorescence microscope and further quantified by FACS analysis [6].

Analysis of fatty acid oxidation (FAO)

The fatty acid oxidation (FAO) rate was evaluated by palmitate oxidation based on previously published methods with minor modifications [10, 11]. In brief, the cells were treated and sub-cultured in T25 flask until 80% confluent, then the cells were then starved in serum free DMEM medium for 2 hrs, then the medium was replaced with DMEM containing 0.5% of BSA, 0.2 mM of cold palmitate and 0.5 μCi/mL of

1-^{14}C-palmitate for another 2 hrs. The flasks were sealed at the beginning of the incubation with a stopper containing a filter (Whatman GF/B paper) pre-soaked in 5% NaOH. The incubation was stopped by the injection of 0.2 ml of 40% perchloric acid into each flask via a needle through the cap to acidify the medium and liberate the CO_2. After overnight isotopic equilibration at room temperature, filters were removed, and the trapped $^{14}CO_2$ and ^{14}C acid-soluble products generated by the oxidation of [^{14}C] palmitate were counted to calculate total palmitate oxidation. The protein concentrations were determined and the results were expressed as nmol per mg proteins per hour (nmol/mg/hr) [12].

De novo lipogenesis

The procedure was based on previously established method with minor modifications [13]. Treated cells were washed and incubated in serum free medium with 100 nM insulin at 37°C overnight. Incubate cells in lipogenesis medium, which including DMEM medium with 100 nM insulin, 10 μM cold acetate and 0.5 μCi ^{3}H-acetate, for 2 hours at 37°C. Cells were then washed and lysed in 120 μl of 0.1 N HCl, and 100 μl of lysates were transferred to 1.5 ml centrifuge tube, and 10 μl of lysates were used for protein assay using Pierce™ BCA Protein Assay Kit (Pierce Biotechnology) per manufacturers' instructions. The lipids were extracted by addition of 500 μl of 2:1 chloroform-methanol (v/v) followed with 5 min incubation at room temperature (RT) after brief vortex. Incubate another 5 min at RT after addition of 250 μl of water with brief vortex. The samples were centrifuged at 3000×g for 10 min at RT. The lower phase was transferred to 4 ml of liquid scintillation fluid, and the ^{3}H activity was determined in scintillation vial and expressed as count per min (cpm).

DNA methylation on ATF4 promoter

The DNA methylation on the ATF4 promoter was evaluated using methylation-specific PCR after bisulfite modification using the below primers. Methylated primer: forward 5'-ttt ttc gtt tat tgc gtt gat atc-3', reverse 5'-taa act tct ata atc aaa atc cgt t-3'; unmethylated primer: forward 5'-ttt ttg ttt att gtg ttg ata ttg g-3', reverse 5'-act aaa ctt cta taa tca aaa tcc att-3'. The product sizes were as follows: 101 bp (methylated) with Tm: 57.2°C & 102 bp (unmethylated) with Tm: 56.0°C; CpG island size: 144 bp; The final methylation results was calculated by normalizing unmethylated input results [7].

Detection of EBV copy number

Genomic DNA was extracted from treated tumor cell lines using a QIAamp DNA Mini Kit (Qiagen). The EBV DNA copy number was measured through qPCR using 50 ng of total DNA with EBV BMRF1 primers (see Table S1), and the results were normalized using cellular β-actin (primers see Table S1) as an internal control [14, 15]. The Namalwa (CVCL_0067) cell line, which contains 2 EBV viral genome copies, was used as a standard to prepare calibration curves for both EBV BMRF1 and β-actin genes, and the EBV viral load was presented as the number of viral genomes per cell [16, 17].

Colony formation in soft agar

This assay is a method for evaluating the ability of individual cell lines to grow in an anchorage-independent manner. Cells were resuspended in DMEM containing 5% FBS with 0.3% agarose and layered on top of 0.5% agarose in DMEM on 60-mm plates. 1000 cells were seeded in 60 mm soft agar dishes for 30 days. The dishes were examined twice per week, and colonies that grew beyond 50 mm in diameter were scored as positive. Each experiment was done in quadruplicate.

In vivo mouse experiments

Balb/c athymic nude male mice (6 weeks old) were obtained from the Guangdong Medical Animal Center. 2×10^6 of viable treated LCL1 cells were washed, harvested in PBS, and then injected into the lateral tail vein in a volume of 0.1 ml. The mice receiving tail vein injections were separated into the following 5 groups (n=9). Group 1 (CTL): cells with empty control (CTL) lentivirus infection; Group 2 (shEBNA2): cells were infected by shEBNA2 lentivirus; Group 3 (shATF4): Cells were infected by shATF4 lenti-

virus; Group 4 (shUSF1): cells were infected by shUSF1 lentivirus; Group 5 (shEBNA2/↑ATF4): cells were infected by shEBNA2 and ATF4 lentivirus in the presence of 10 μg/ml puromycin.

Mice were monitored for changes in body weight and sacrificed when values fell below 20% of their initial weight. The survival curve was calculated and the final tumor tissues were isolated for biological assays. The lungs of sacrificed mice were isolated and fixed in 10% formalin and the number of surface metastases per lung was determined under a dissecting microscope. Parts of the tumor tissues were fixed in 4% buffered formaldehyde, paraffin embedded, and sectioned to 4 mm thickness before they were then processed for H&E staining. Images were taken using a Carl Zeiss MIRAX MIDI slide scanner and analyses were performed using a 3DHISTECH Pannoramic Viewer. Parts of the tumor tissues were isolated for *in vivo* monitoring of superoxide anion release; gene expression, including mRNA and protein levels were determined.

In vivo superoxide anion ($O_2^{\cdot-}$) release

Superoxide anion release in amygdala tissues were extracted by dimethyl sulfoxide-tetrabutylammonium chloride (DMSO-TBAC) solution and the TBAC-$O_2^{\cdot-}$ complex was then further detected by use of the luminol-EDTA-Fe enhanced chemiluminescence system [18]. Briefly, the biological tissues were isolated and purged continuously by N2 gas to remove traces of oxygen, and $O_2^{\cdot-}$ from tissues was extracted by DMSO-TBAC, then the chemiluminescent reagents and $O_2^{\cdot-}$ extract solutions were pumped into a glass scintillation vial which was placed in the luminometer, and the chemiluminescence intensity was continuously monitored for 2 min and calculated. Superoxide levels were calculated from the standard curve generated by the xanthine/xanthine oxidase reaction [6].

Statistical analysis

The data was given as mean ± SD (standard deviation); all of the experiments were performed at least in quadruplicate unless otherwise indicated. One-way analysis of variance (ANOVA) followed by the Turkey-Kramer test was used to determine statistical significance of different groups. The mouse survival curve was determined through Kaplan-Meier survival analysis using SPSS 22 software, and a P value <0.05 was considered significant.

References

[1] Bodnar AG, Ouellette M, Frolkis M, Holt SE, Chiu CP, Morin GB, Harley CB, Shay JW, Lichtsteiner S and Wright WE. Extension of life-span by introduction of telomerase into normal human cells. Science 1998; 279: 349-52.

[2] Kong D, Zhan Y, Liu Z, Ding T, Li M, Yu H, Zhang L, Li H, Luo A, Zhang D, Wang Y, Wang S, Zhang Z, Zhang H, Huang X, Yao P, Ding Y and Liu Z. SIRT1-mediated ERbeta suppression in the endothelium contributes to vascular aging. Aging Cell 2016; 15: 1092-102.

[3] Yu H, Zhang H, Chu Z, Ruan Q, Chen X, Kong D, Huang X, Li H, Tang H, Wu H, Wang Y, Xie W, Ding Y and Yao P. Combination of betulinic acid and chidamide synergistically inhibits Epstein-Barr virus replication through over-generation of reactive oxygen species. Oncotarget 2017; 8: 61646-61.

[4] Lan K, Verma SC, Murakami M, Bajaj B and Robertson ES. Epstein-Barr Virus (EBV): infection, propagation, quantitation, and storage. Curr Protoc Microbiol 2007; Chapter 14: Unit 14E.2.

[5] Ceradini DJ, Yao D, Grogan RH, Callaghan MJ, Edelstein D, Brownlee M and Gurtner GC. Decreasing intracellular superoxide corrects defective ischemia-induced new vessel formation in diabetic mice. J Biol Chem 2008; 283: 10930-8.

[6] Yao D, Shi W, Gou Y, Zhou X, Yee Aw T, Zhou Y and Liu Z. Fatty acid-mediated intracellular iron translocation: a synergistic mechanism of oxidative injury. Free Radic Biol Med 2005; 39: 1385-98.

[7] Zou Y, Lu Q, Zheng D, Chu Z, Liu Z, Chen H, Ruan Q, Ge X, Zhang Z, Wang X, Lou W, Huang Y, Wang Y, Huang X, Liu Z, Xie W, Zhou Y and Yao P. Prenatal levonorgestrel exposure induces autism-like behavior in offspring through ERbeta suppression in the amygdala. Mol Autism 2017; 8: 46.

[8] Zhang H, Li L, Chen Q, Li M, Feng J, Sun Y, Zhao R, Zhu Y, Lv Y, Zhu Z, Huang X, Xie W, Xiang W and Yao P. PGC1beta regulates multiple myeloma tumor growth through LDHA-mediated glycolytic metabolism. Mol Oncol 2018; 12: 1579-95.

[9] Zhang H, Li L, Li M, Huang X, Xie W, Xiang W and Yao P. Combination of betulinic acid and chidamide inhibits acute myeloid leukemia by suppression of the HIF1alpha pathway and generation of reactive oxygen species. Oncotarget 2017; 8: 94743-58.
[10] Taib B, Bouyakdan K, Hryhorczuk C, Rodaros D, Fulton S and Alquier T. Glucose regulates hypothalamic long-chain fatty acid metabolism via AMP-activated kinase (AMPK) in neurons and astrocytes. J Biol Chem 2013; 288: 37216-29.
[11] Huynh FK, Green MF, Koves TR and Hirschey MD. Measurement of fatty acid oxidation rates in animal tissues and cell lines. Methods Enzymol 2014; 542: 391-405.
[12] Li H, Liu Z, Gou Y, Yu H, Siminelakis S, Wang S, Kong D, Zhou Y, Liu Z, Ding Y and Yao D. Estradiol mediates vasculoprotection via ERRα-dependent regulation of lipid and ROS metabolism in the endothelium. J Mol Cell Cardiol 2015; 87: 92-101.
[13] Akie TE and Cooper MP. Determination of fatty acid oxidation and lipogenesis in mouse primary hepatocytes. J Vis Exp 2015; e52982.
[14] Verma D, Thompson J and Swaminathan S. Spironolactone blocks Epstein-Barr virus production by inhibiting EBV SM protein function. Proc Natl Acad Sci U S A 2016; 113: 3609-14.
[15] Zuo L, Yu H, Liu L, Tang Y, Wu H, Yang J, Zhu M, Du S, Zhao L, Cao L, Li G and Lu J. The copy number of Epstein-Barr virus latent genome correlates with the oncogenicity by the activation level of LMP1 and NF-kappaB. Oncotarget 2015; 6: 41033-44.
[16] Hui KF and Chiang AK. Suberoylanilide hydroxamic acid induces viral lytic cycle in Epstein-Barr virus-positive epithelial malignancies and mediates enhanced cell death. Int J Cancer 2010; 126: 2479-89.
[17] Rose C, Green M, Webber S, Kingsley L, Day R, Watkins S, Reyes J and Rowe D. Detection of Epstein-Barr virus genomes in peripheral blood B cells from solid-organ transplant recipients by fluorescence in situ hybridization. J Clin Microbiol 2002; 40: 2533-44.
[18] Yao D, Vlessidis AG, Gou Y, Zhou X, Zhou Y and Evmiridis NP. Chemiluminescence detection of superoxide anion release and superoxide dismutase activity: modulation effect of Pulsatilla chinensis. Anal Bioanal Chem 2004; 379: 171-7.

Table S1. Sequences of primers for the real time quantitative PCR (qPCR)

Gene	Species	Analysis	Forward primer (5'→3')	Reverse primer (5'→3')
EBNA2	EBV	mRNA	ggagtcccataatagcccaga	actgggtccctccacataatc
β-actin	Human	Genome	ctggacttcgagcaagagatg	aggaaggaaggctggaagagt
BMRF1	EBV	Genome	ccgtcctgtccaagtgctat	gggagacctcgaagctgatta
β-actin	Human	mRNA	gatgcagaaggagatcactgc	atactcctgcttgctgatcca
ATF4	Human	mRNA	ccccttcaccttcttacaacc	gatcatggcaacgtaagcagt
USF1	Human	mRNA	gcagcagaaaacagctgaaac	tcggaagacgtacttgacgtt
SREBP1	Human	mRNA	ccacattgagctcctctcttg	tggcactgactcttccttgat
ChREBP	Human	mRNA	agacagcaacaagaccgagaa	gtggtagctttgctcaccttg
FAS	Human	mRNA	acagggacaacctggagttct	ctgtggtcccacttgatgagt
ATF4	Human	ChIP	ccttttctcgtcacagctacg	cggccctttatagacttcgtc

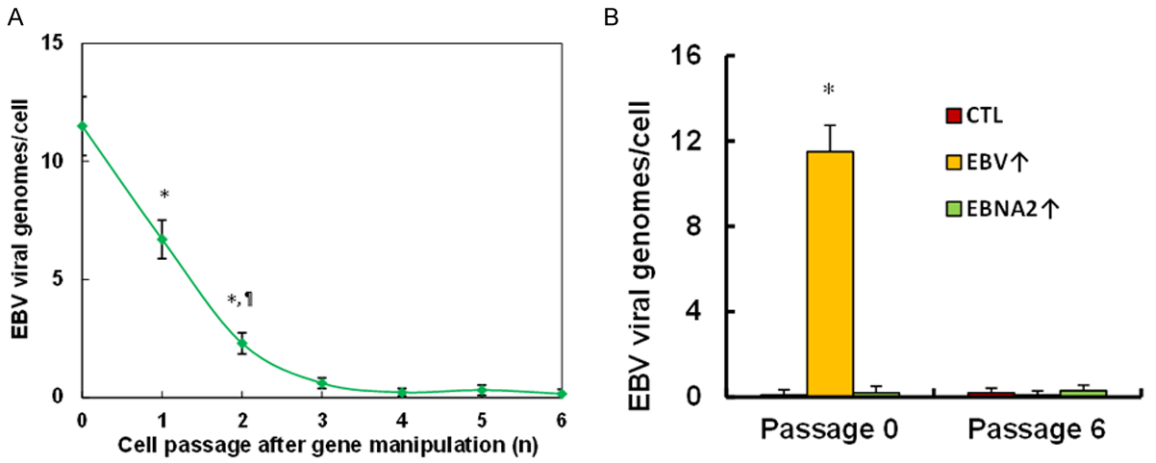

Figure S1. EBV virus diminished quickly after virus infection in HBL cells. A. Curves of EBV genomic copies from passage 0 to 6. *, $P<0.05$, vs Passage 0; ¶, $P<0.05$, vs Passage 1. B. EBV genomic copies at passage 0 and 6. *, $P<0.05$, vs CTL group.

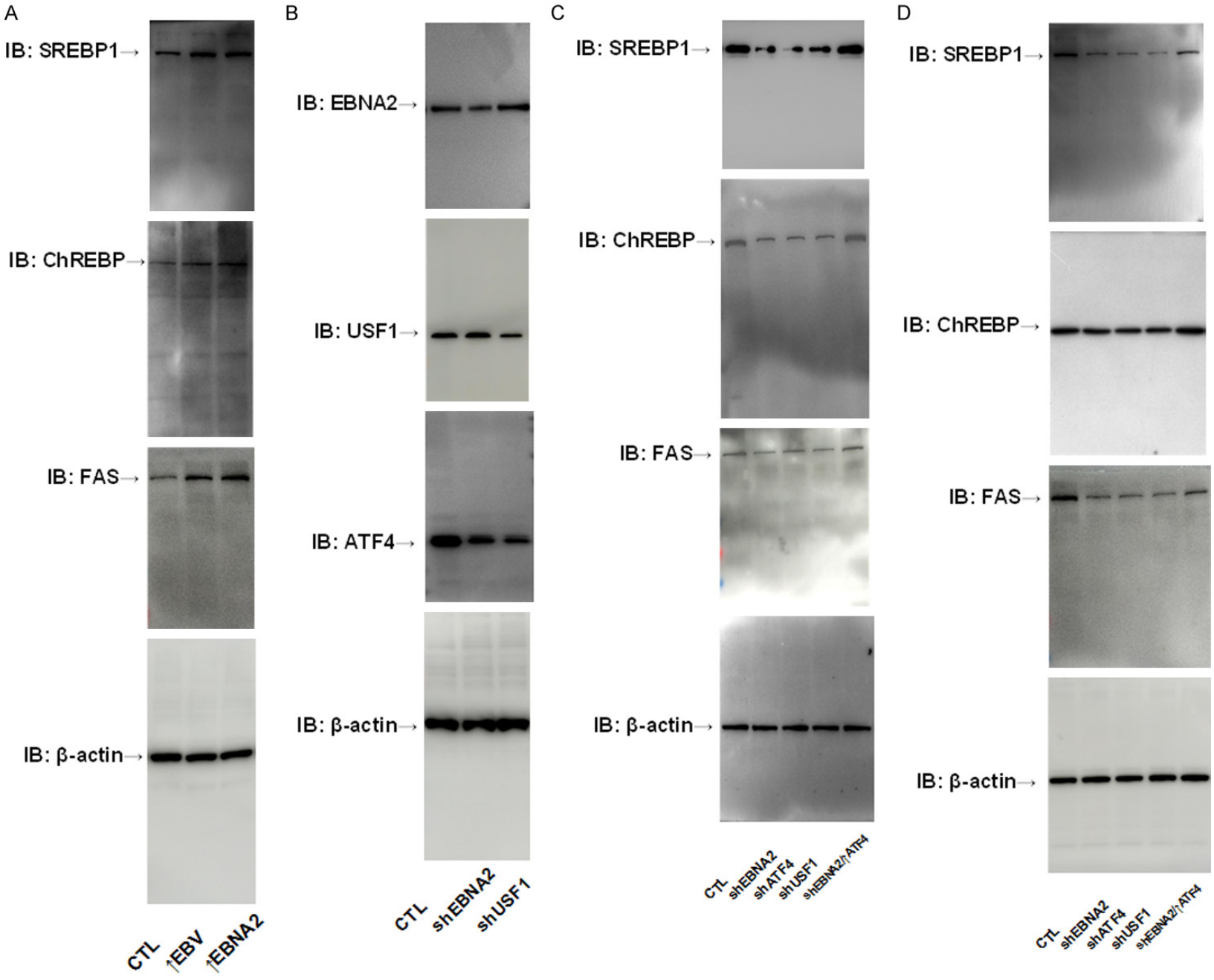
A
IB: SREBP1→
IB: ChREBP→
IB: FAS→
IB: β-actin→
CTL
↑EBV
↑EBNA2
B
IB: EBNA2→
IB: USF1→
IB: ATF4→
IB: β-actin→
CTL
shEBNA2
shUSF1
C
IB: SREBP1→
IB: ChREBP→
IB: FAS→
IB: β-actin→
CTL
shEBNA2
shATF4
shUSF1
shEBNA2/ATF4
D
IB: SREBP1→
IB: ChREBP→
IB: FAS→
IB: β-actin→
CTL
shEBNA2
shATF4
shUSF1
shEBNA2/ATF4

Figure S2. Representative full blots for Western Blotting. A. Representative full blots for **Figure 1E**. B. Representative full blots for **Figure 2F**. C. Representative full blots for **Figure 3E**. D. Representative full blots for **Figure 6C**.

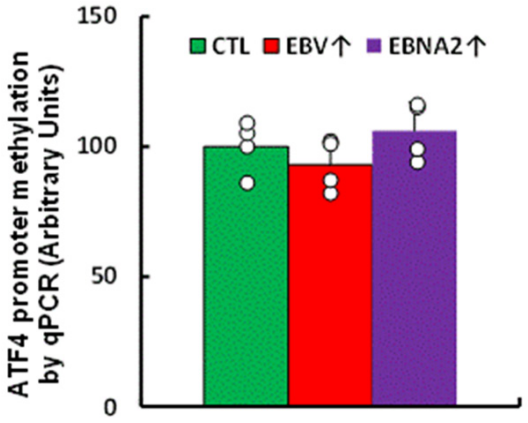

Figure S3. Exposure of EBV or EBNA2 does not change the DNA methylation on the ATF4 promoter. HBL were infected by either control (CTL), EBV virus (↑EBV) or EBNA2 lentivirus (↑EBNA2) for DNA methylation assay on the ATF4 promoter.